

Review

# PIXE and Its Applications to Elemental Analysis

Keizo Ishii <sup>1,2</sup>

<sup>1</sup> Cyclotron and Radioisotope Center, Tohoku University, Aoba-ku, Aramaki, Aza-Aoba 6-3, Sendai 980-0845, Japan; keizo.ishii@qse.tohoku.ac.jp; +81-22-795-7800

<sup>2</sup> Tohoku Radiation Science Center, Aoba-ku chuo 2-8-13, Sendai 980-0021, Japan

Received: 21 April 2019; Accepted: 4 June 2019; Published: 10 June 2019



**Abstract:** When charged particles collide with atoms, atomic inner shell electrons become ionized, producing characteristic X-rays. This phenomenon is called particle-induced X-ray emission (PIXE). The characteristic X-ray production cross-sections from PIXE are very large, and the characteristic X-rays of elements contained in a sample are easily measured by a Silicon detector with a high energy resolution. Hence, sodium to uranium can be detected with a sensitivity of ppb~ppm, and PIXE has been applied to trace element analysis. Scanning ion beams can be used to obtain the spatial distributions of elements in a sample. Furthermore, the distributions of elements inside a cell can be investigated using micro ion beams. PIXE analysis is a very useful technique for multi-elemental analysis and is now widely used in many fields and applications, including chemistry, medicine, biology, archaeology, agriculture, materials science, fisheries science, geology, petrology, environmental study, contamination monitoring, resource search, semiconductors, metal, astrophysics, earth science, criminal investigations, and food.

**Keywords:** PIXE; particle-induced X-ray emission; inner shell ionization; atomic bremsstrahlung; trace element analysis; micro-beams; micro-PIXE analysis

---

## 1. Introduction

When heavy charged particles, on the order MeV, bombard target atoms, characteristic X-rays of the target atoms are produced. This phenomenon is called particle-induced X-ray emission (PIXE) [1]. Figure 1 shows the X-ray spectrum of the Ti target bombarded with 3 MeV  $\alpha$  particles. Since the continuous background appearing in the X-ray energy spectrum obtained by heavy charged particle bombardment is much smaller than that of the electron bombardment, PIXE can be used for trace element analysis. This is called PIXE analysis [1] in which protons and  $\alpha$  particles are usually used. This type of analysis has been widely applied to chemistry, medicine, biology, agriculture, fisheries, industry, environmental pollution, archeology, criminal investigations, and searches for mineral resources.

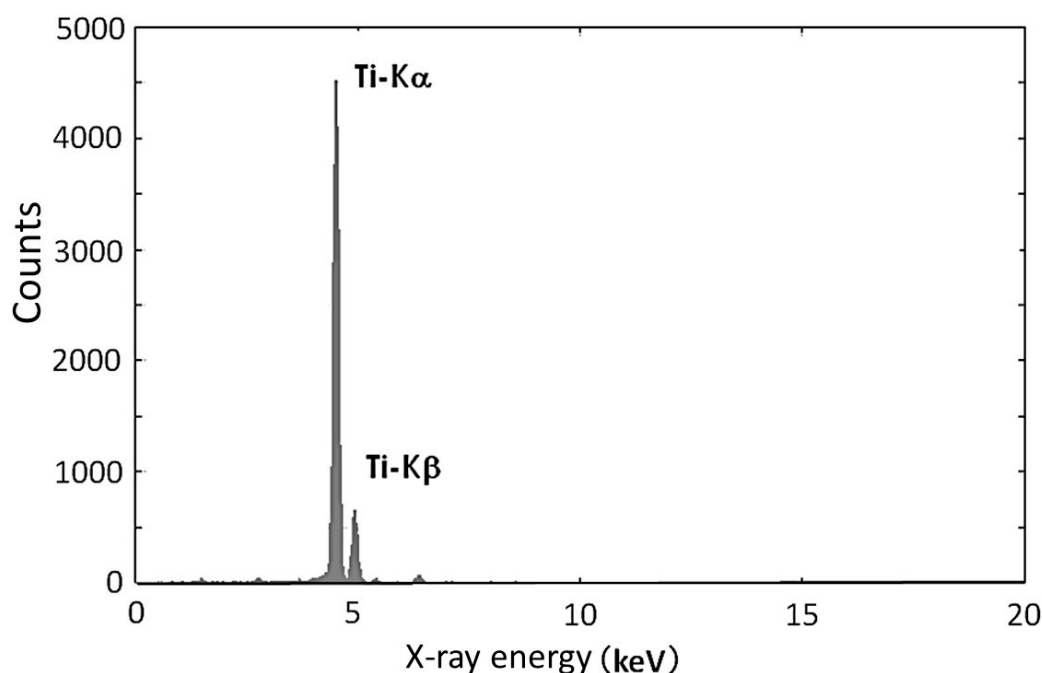


**Figure 1.** X-ray energy spectrum of a Ti target bombarded with 3 MeV  $\alpha$  particles.

Generally, the results of quantitative analysis are affected by the chemical treatment of the sample. For example, in the case of the inductively coupled plasma-mass spectrometry (ICP-MS) modality, the chemical state of the sample may affect the atom ionization [2]. However, in the case of PIXE analysis, the sample can be analyzed directly, and the quantities of elements can be deduced in a straightforward manner. Moreover, scanning proton beams can be used to investigate the distribution of elements on the surface of the sample. Micro-beams can be used to research the inner parts of cells [3].

The history of PIXE research is long. The technology was first developed by physicists in the 1950s, and it was applied in the 1970s and 1980s. The first international conference on “PIXE and its applications” was organized in 1970 by S.A.E. Johansson, a professor at the Lund Institute of Technology in Lund, Sweden. This conference continues to this day. Most of the technologies related to PIXE analysis were completed by the 1980s. Johansson published a textbook on PIXE analysis with Professor J. L. Campbell in 1988 [3]. The International Journal of PIXE (World Scientific) for PIXE was published in 1991 by the efforts of S. Morita, a professor at Tohoku university in Sendai, Japan, with the cooperation of Prof. S.A.E. Johansson. Under the background of high activity of biological applications, the first international symposium on “Bio-PIXE” was held at Tohoku university in Sendai 1992, and this symposium also continues to this day.

Tohoku University has focused intensely on basic and applied PIXE research, from the first stage of PIXE development. In this paper, we introduce inner shell ionization in ion-atom collisions, the X-ray production associated with this ionization, PIXE analysis, and its applications based on the research mainly carried out at Tohoku university.

## 2. Inner Shell Ionization Due to Bombardment with Heavy Charged Particles

Inner shell ionization is classified into three types based on the velocity of the projectile. In the case that such a projectile velocity is smaller than or the same as the average velocity of the inner shell electrons, the inner shell electrons are ionized by close collisions with heavy charged particles, which is known as Rutherford scattering. In the case that the projectile velocity is larger than the average velocity of the inner shell electrons, the inner shell electrons are ionized by distant collisions, where the electrons interact with the projectile as a cloud. In the case such that the projectile velocity is close

to the speed of light, the inner shell electrons are ionized by the photoelectric effect induced by the virtual photons.

First, we consider binary collisions between projectiles and target electrons. The mass of the electron and that of the projectile are expressed as  $m_e$  and  $m_p$ , respectively. The target electron is bound in an atom with energy ( $= -U = \frac{1}{2}m_e v^2 - \frac{Ze^2}{r}$  where  $U, r, v, Z$  and  $e$  are the binding energy, distance from the nucleus, velocity of the electron at  $r$ , atomic number, and elementary charge, respectively). In the case of a head-on collision between a projectile with velocity  $V$  and an electron, the transfer energy from the projectile to the electron is  $2m_e V^2 + 2m_e vV$ . The ionization condition is  $2m_e V^2 + 2m_e vV > U$  ( $v > (U - 2m_e V^2)/(2m_e V)$ ). Electrons with large velocities are only ionized in the case of low velocity projectiles in the vicinity of the nucleus. Therefore, the inner shell ionization cross sections drop with decreasing projectile energy  $E (= m_p V^2/2)$ , which is approximately proportional to  $E^4$ . Under the condition of  $2m_e V^2 > U$  :  $E > 4m_p U/m_e$ , all of the electrons can be ionized, and the ionization cross sections are maximized at  $E = m_p U/m_e$ . Above this projectile energy, the ionization cross sections decrease as a function of  $1/E$ . Figure 2 shows the K-shell ionization cross sections of Al as a function of proton energy. The reason for the maximum at  $E = m_p U/m_e$  is as follows: According to the Virial theorem, the relationship between the average kinetic energy  $\bar{T} \equiv \langle m_e v^2/2 \rangle$  and the average potential energy  $\bar{V} \equiv \langle Ze^2/r \rangle$  is obtained by  $\bar{T} = \bar{V}/2$ . This result gives  $\bar{T} = U$  due to the identity  $-U = \bar{T} - \bar{V}$ . The existence probability of the electron is maximized at the average radius of the electron orbital. The ionization probability peaks when the projectile reaches this position. Considering the uncertainty principle,  $\Delta x \Delta p \geq \hbar/2$ , and adopting the orbital radius  $na_0/Z$  as  $\Delta x$  and the minimum transfer momentum from the projectile to the bound electron  $\sqrt{2m_p E} - \sqrt{2m_p(E-U)} \approx \sqrt{m_p U^2/2E}$  as  $\Delta p$ , we obtain the expression  $(na_0/Z) \sqrt{m_p U^2/2E} \approx \hbar/2$ . Assuming  $U = Z^2 Ry/n^2$ , where  $Ry$  is the Rydberg constant and  $n$  is the principal quantum number, we obtain  $E = m_p U/m_e$ . This implies that the ionization cross sections are maximized when the projectile velocity becomes the same as the average velocity of the bound electron.

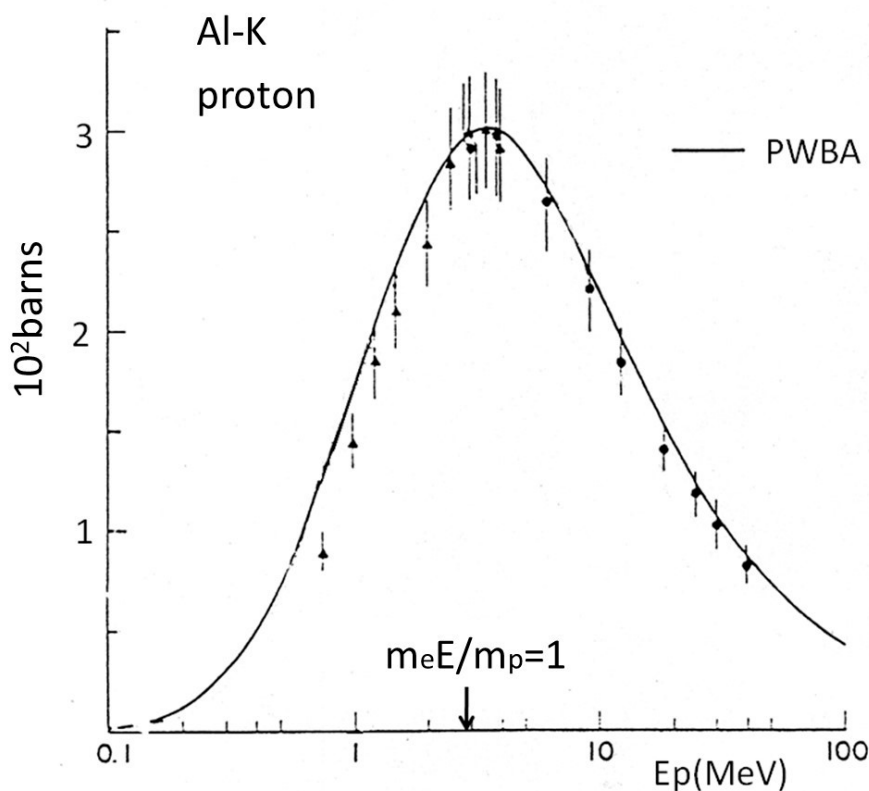


Figure 2. K-shell ionization cross sections of Al as a function of proton energy.

The inner shell ionization cross sections  $\sigma^i$  can be estimated by using the binary encounter approximation, based on Rutherford scattering between the electron and the projectile, and by using the velocity distribution calculated classically, taking into consideration the inner shell electron being bound by the Coulomb potential of the target nucleus [4]. This theory expresses  $\sigma^i$  as the function of  $m_e E / m_p U$ ,

$$U^2 \sigma^i(E, U) / z^2 = f(m_e E / m_p U) \quad (1)$$

where  $z$  is the charge of the projectile. This is called the scaling law for inner shell ionization cross sections.

In the case of ion-atom collision, the projectile can simultaneously ionize several inner shell electrons. This phenomenon is called multiple-inner shell ionization. For example, K-shell and L-shell multiple ionization is indicated by the satellite lines at  $K_\alpha$  and  $K_\beta$  X-rays in the X-ray energy spectrum. The probability of multiple inner shell ionization as a function of the impact parameter can be estimated by perturbation theory, based on a semi-classical approximation [5] where the projectile is treated as an electric field. The distribution of satellite lines is binomial.

The first theoretical calculation for inner shell ionization cross sections by heavy charged particles was carried out using the plane wave Born approximation [6]. The cross sections of the K-shell of Al are shown in Figure 2. There is a discrepancy between the experimental values and theoretical predictions in the low projectile energy region. This can be explained by the effects of Coulomb deflection of the projectile and the increased binding energy of the inner shell electrons due to the Coulomb field of the projectile. An approximation including these effects was derived by Brandt et al. [7] and was further improved as CPPR-PWBA [8]. This approximation reproduces the experimental cross sections of inner shell ionizations to within 5% and is typically used in quantitative analysis [9]. The inner shell ionization cross sections by heavy charged particles were measured energetically in the 1970s and converted into a table in the 1980s [10].

### 3. X-ray Production by Heavy Charged Particle Impacts

When an unoccupied state produced by inner shell ionization due to heavy charged particle impacts is filled by an outer shell electron, a characteristic X-ray or Auger electron is emitted. The  $K_\alpha$  and  $K_\beta$  X-ray lines in Figure 1 indicate the transitions to the K-shell from the L-shells and M-shells, respectively. We denote the transition probabilities of the  $K_\alpha$  X-rays,  $K_\beta$  X-rays, and Auger electrons [11] as  $\Gamma_\alpha^X, \Gamma_\beta^X$ , and  $\Gamma^A$ , respectively. The emission ratio of X-ray  $\omega$  is defined by the equation below.

$$\omega = \frac{\Gamma_\alpha^X + \Gamma_\beta^X}{\Gamma_\alpha^X + \Gamma_\beta^X + \Gamma^A} \quad (2)$$

$\omega$  is called the fluorescence yield [12]. This value is small in the case of lighter elements.

The total production cross sections of  $K_\alpha$  and  $K_\beta$  X-rays are expressed by the equations below.

$$\sigma_{K_\alpha}^X = \frac{\Gamma_\alpha^X}{\Gamma_\alpha^X + \Gamma_\beta^X} \omega_K \sigma^i_{K_\alpha}, \quad \sigma_{K_\beta}^X = \frac{\Gamma_\beta^X}{\Gamma_\alpha^X + \Gamma_\beta^X} \omega_K \sigma^i_{K_\beta} \quad (3)$$

The total production cross sections of  $L_\alpha$ -X-rays,  $L_\beta$ -X-rays, and  $L_\gamma$ -X-rays are derived in a similar manner. L-X lines are complicated when compared to the K-X lines. In the case of projectile energies lower than 1 MeV, the differential production cross sections of L X-rays are slightly dependent on the emission angle in the direction in which the projectiles are incident [13], whereas those of K X-rays are isotropic.

In addition to the characteristic X-rays, continuous X-rays are produced in ion-atom collisions. There are three processes for the production of continuous X-rays: quasi-free electron bremsstrahlung (QFEB) [14], secondary electron bremsstrahlung (SEB) [15], and atomic bremsstrahlung (AB) [16].

QFEB is the target electron bremsstrahlung produced by the Coulomb potential of the projectile and is the main component of the continuous X-ray energy spectrum for values less than  $m_e E/m_p$ . The secondary electrons are ejected from atoms in the inner shell ionization. SEB is produced by the Coulomb potentials of the target nuclei and is the main component of the continuous X-ray energy spectrum for values less than  $4m_e E/m_p$ . AB is the inner shell electron bremsstrahlung produced by the Coulomb potential of the target nucleus, without ionization during ion atom collisions, and becomes the main component of the continuous X-ray energy spectrum for values larger than  $4m_e E/m_p$ . These continuous X-rays form the continuous background in the X-ray energy spectrum obtained from PIXE analysis.

#### 4. Applications of PIXE to Elemental Analysis

We adjusted the beam spot size to approximately 1 mm, with slits or a collimator placed just before the target, and measured the X-rays from the target using an X-ray detector. The X-ray energy spectrum was stored on a personal computer and the counts  $N_X(Z)$  of the characteristic X-rays for an element (atomic number  $Z$ ) were obtained. Mounting a sample uniformly on a thin polyethylene film, we obtain the quantity  $N_Z(g/cm^2)$  for element  $Z$  as follows.

$$N_Z = N_X(Z) \frac{4\pi m_Z Z_p e}{\sigma_Z^X d\Omega eff_Z Q N_{Av}} \quad (4)$$

where  $d\Omega$ ,  $eff_Z$ ,  $Q$ ,  $Z_p$  and  $N_{Av}$  are the solid angle of the X-ray detector, the detector efficiency, integrated projectile charge, projectile charge, and Avogadro's number, respectively. In the case of a thick target, the effect of the reduction due to the X-ray self-absorption and projectile energy loss in the target should be considered when applying the above formula.

We typically use the internal standard method for quantitative analysis. Mixing a standard element,  $A$ , in a known amount,  $N_A$ , into the sample, we obtain the following formula for an unknown amount,  $N_Z$ .

$$N_Z = N_A \frac{N_X(Z)}{N_X(A)} \frac{m_Z \sigma_A^X eff_A}{m_A \sigma_Z^X eff_Z} \quad (5)$$

The external standard method is applied by making a standard target containing  $A$ , in the known amount,  $N_A$ , and then measuring the X-rays from the sample target and the standard target independently. The quantitative formula is shown below.

$$N_Z = N_A \frac{N_X(Z)}{N_X(A)} \frac{m_Z \sigma_A^X eff_A Q_A}{m_A \sigma_Z^X eff_Z Q_Z} \quad (6)$$

Electron-impacts can also produce the characteristic X-rays. However, the electron bremsstrahlung of the electron beams themselves are intensively emitted by the sample. The intensity of this bremsstrahlung is approximately 1000 times the SEB. Therefore, electron beams are not appropriate for trace element analysis [17].

Proton beams are generally used for PIXE analysis due to the low energy loss in the sample. The detection limit of PIXE analysis is determined by the background of the X-ray spectrum. The main background produced by proton impacts of less than 1.5 MeV, 1.5–2 MeV, and larger than 3MeV is AB, AB + SEB, and SEB + Compton tail background of  $\gamma$ -rays, respectively [18]. Figure 3 shows the two-dimensional expression of the detection limit estimated based on these backgrounds in the case of a biological sample [19]. We can see from this figure that an appropriate proton energy for PIXE analysis is approximately 3 MeV.

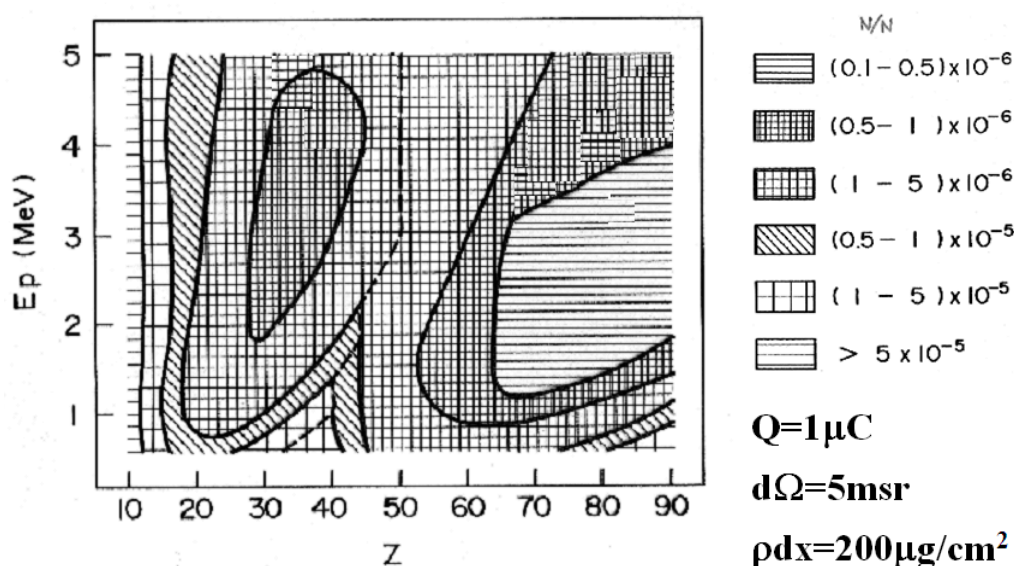


**Figure 3.** Detection limit of particle-induced X-ray emission (PIXE) analysis for biological samples.

### 5. Accelerators Used in PIXE Analysis

As shown in Figure 3, a small electrostatic accelerator or small cyclotron for accelerating protons to energies of a few MeV is appropriate for PIXE analysis. Tandem electrostatic accelerators, such as the Tandatron accelerator and Pelletron tandem accelerator, have been widely used. A single-ended Van de Graaff accelerator of a small beam emittance can form a micro-beam spot on the target by using strongly convergent quadrupole magnets and slits.

A cyclotron is mainly used to accelerate heavy charged particles of more than 10 MeV. Recently, positron emission tomography (PET) using a positron emitter nuclide has become popular for functional diagnostic imaging. Accelerators of several tens of MeV are required to produce positron emitter nuclides. When accelerating hydrogen molecules instead of deuterons under the cyclotron acceleration mode condition for 6 MeV deuterons, proton beams of 3 MeV can be obtained. There is an institution that uses such proton beams for PIXE analysis [20]. Furthermore, a compact cyclotron (3 MeV proton beams) has been developed for applications to PIXE analysis [21]. A PIXE analysis method using proton beams of energies greater than 10 MeV from a cyclotron has also been developed [22]. However, the sensitivity is lower than that of the 3 MeV protons.

### 6. X-ray Detector for PIXE Analysis

PIXE can be applied to trace element analysis due to the successful development of a high resolution X-ray detector known as a Si(Li) detector [3]. Due to the thick detection length, it can measure the K X-rays of uranium. The energy resolution of this detector was approximately 220 eV, which was achieved by cooling FET circuits with liquid nitrogen and characteristic X-rays for almost all elements, which were observed separately in the PIXE spectrum. The size of this detector was large due to the liquid nitrogen cooling system. Recently, a silicon drift detector (SDD) has been developed, from which a high energy resolution 125–140 eV can be obtained due to the Peltier cooling effect. The size of this detector is small, which makes it easy to use when compared to the previous version. However, the detection length is approximately 0.5 mm and the efficiency is low for higher atomic number elements. The CdTe detector is useful for high atomic number elements. These X-ray detectors are already marketed commercially.

### 7. Target Preparation for PIXE Analysis

We prepared a target frame made from polypropylene with a hole diameter of 25 mm at the center. We then placed a thin backing film consisting of hydrogen and carbon into the frame. The

detection sensitivity increases because the backing film is thin. Dropping polyvinyl formal liquid onto the surface of grape sugar liquid and then peeling up the thin film that forms on the surface can be used to make a backing film with a thickness of approximately  $0.1 \mu\text{m}$  [23]. We can also make an ultra-thin backing film by vapor-depositing high-purity carbon. When the PIXE analysis method was initially developed, the aim was to achieve ultra-trace element analysis. These films proved very useful to that end. At present, it is common to use a polypropylene film with a thickness of  $4 \mu\text{m}$ , which is comparatively high strength and easy to use.

Usually, we homogenize a sample, drop it onto the backing film, dry it, irradiate it with proton beams, measure X-rays, and perform the PIXE analysis. The sensitivity of PIXE analysis can be improved by liquefying the sample by adding nitric acid and transpiring water with a microwave oven [24]. However, halogen elements are evaporated when applying this method.

When the sample is water, passing through a charcoal filter and then incinerating the charcoal filter enables us to condense the sample and raise the sensitivity to ppt [25].

In the case of mineral samples, there is a simple method in which the sample is powdered in an agate bowl, mixed with glycerin, and smeared on a backing film.

## 8. Target Chamber for PIXE Analysis

A vacuum chamber is usually used for PIXE analysis. The inner wall surface of the chamber is covered with polyethylene resin film with a thickness of 1 mm to protect the scattered beams. The beam collimators to the target should be designed to ensure that halo beams do not hit the target frame.

The proton beams can be extracted from the vacuum to the atmosphere by passing through a Kapton film with a thickness of  $10 \mu\text{m}$ , and the PIXE analysis can be carried out under atmospheric conditions [26]. Ar elements in the air can be used as the standard element.

## 9. Peak Separation Methods in PIXE Analysis

The peaks of the characteristic X-rays for each element appearing in the X-ray energy spectrum are fitted to Gaussian functions by the least squares method and X-ray counts are obtained with respect to the peaks. Figure 4 shows an example of peak separation in an X-ray energy spectrum of bovine liver obtained using 3 MeV proton PIXE [27].

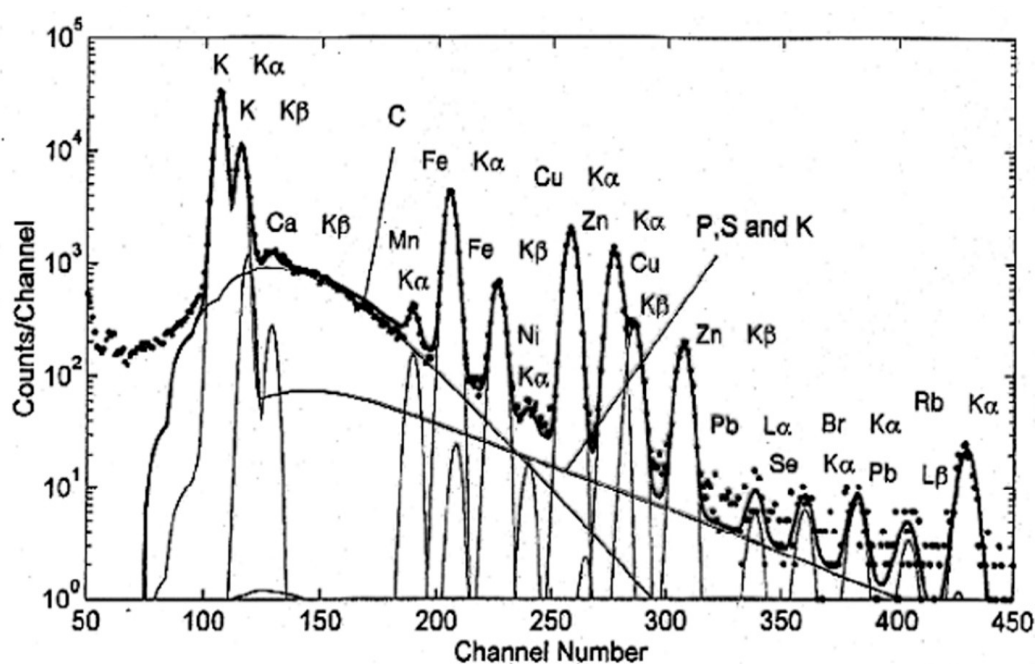


Figure 4. Peak separation of an X-ray energy spectrum of bovine liver obtained using 3 MeV proton PIXE.

The continuous background in this figure consists of SEB and AB from carbon, phosphorus, sulfur and potassium.

Peak fitting software is commercially available, such as GUPIXWIN (University of Guelph, Guelph, ON, Canada).

## 10. Applications of PIXE Analysis

Because the PIXE analysis method is simple and can be used to analyze almost all elements simultaneously with high sensitivity, it is now used in a broad range of fields and applications, such as contamination monitoring of food, materials science, medicine, biology, fisheries, agriculture, geology, petrology, environmental study, archaeology, resource searching, semiconductors, metals, chemistry, astrophysics, earth science, and criminal investigations.

### 1. Food

The sensitivity of PIXE analysis to hydrogen, carbon, nitrogen, and oxygen is very low due to absorption in the detection window (usually Be film) of X-ray detectors. However, it is very high in the case of absorption of metallic elements and heavy elements in biological samples consisting of light elements as the main ingredients. Therefore, PIXE is suitable for analyzing biological samples. Research on food inspection swiftly followed the development of PIXE analysis. Figure 5 shows the PIXE spectrum of canned tomato juice [28].

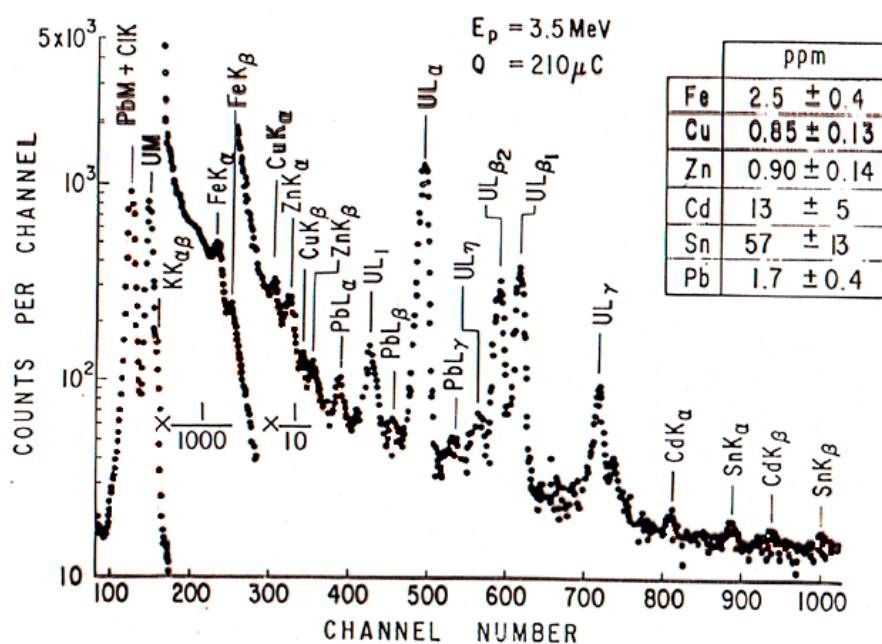


Figure 5. Analysis of canned tomato juice.

The sample was contaminated with uranium as the standard element. We can see from the spectrum that the sample contained poisonous elements such as Cd, Sn, and Pb. Because solder was used for junctions of tin plates for canned tomato juice sold in the early 1970s, the juice was contaminated with tin.

### 2. Biological Sample

A blood sample can easily be analyzed by extracting a small quantity from the body and placing it on a thin film. Figure 6 shows the X-ray energy spectrum of a healthy person's blood.

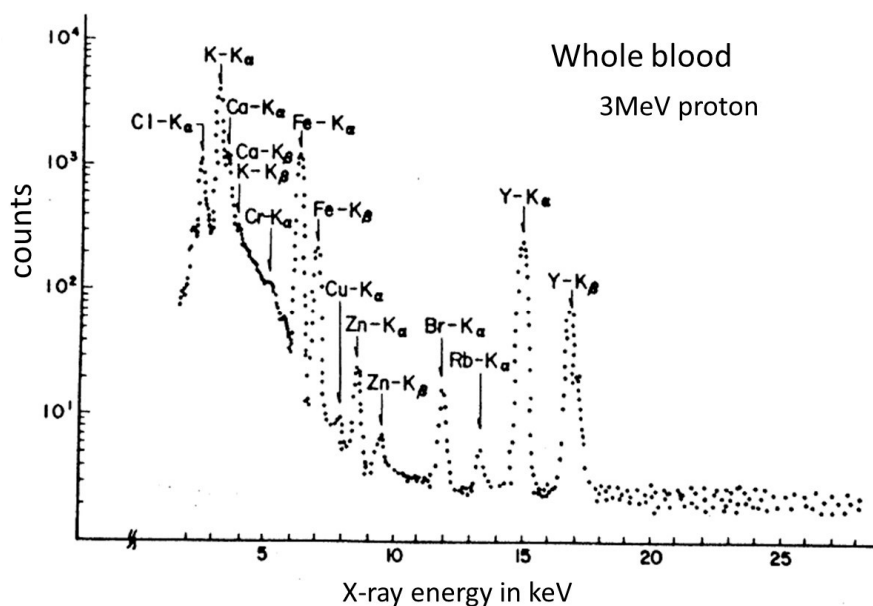


Figure 6. The PIXE spectrum of the whole blood of a healthy person.

The peaks of the elements Na, P, S, K, Cl, Ca, Cr, Fe, Cu, Zn, Br, and Y were observed in this spectrum. The Y element was contaminated in the sample as a standard element. Research based on PIXE analysis has revealed that changes in the concentrations of metallic elements in the blood are strongly related to aging and illness. Since changes in the concentration of Zn are strongly related to disease, the results of PIXE analysis may be useful for diagnosing certain health conditions. It seems that the concentration ratio, Cu/Zn, of Cu and Zn in blood is also closely related to health conditions. The results of PIXE analysis in the blood of leukemia patients showed that the concentration ratio of Cu/Zn was four times larger than that of normal people. It has also been reported that chronic articular rheumatism affects the concentration ratios of elements [29].

### 3. Air Sample

PIXE analysis of airborne dust has been carried out for many years and has contributed to the prevention of environmental destruction by air pollution. Dust in the atmosphere is collected using an aerosol sampler with a nucleopore membrane filter, which contains many small holes and is used as a backing film for PIXE analysis. Figure 7 shows the results of PIXE analysis of airborne dust collected from Sapporo, Japan in April 1982 [30].

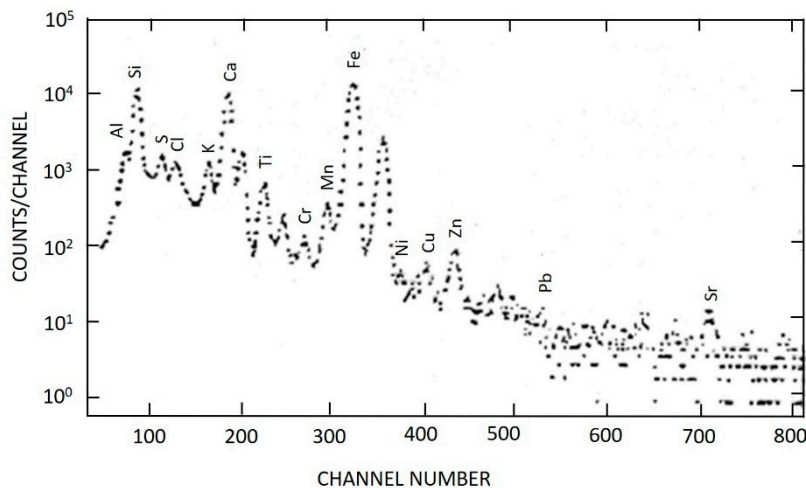
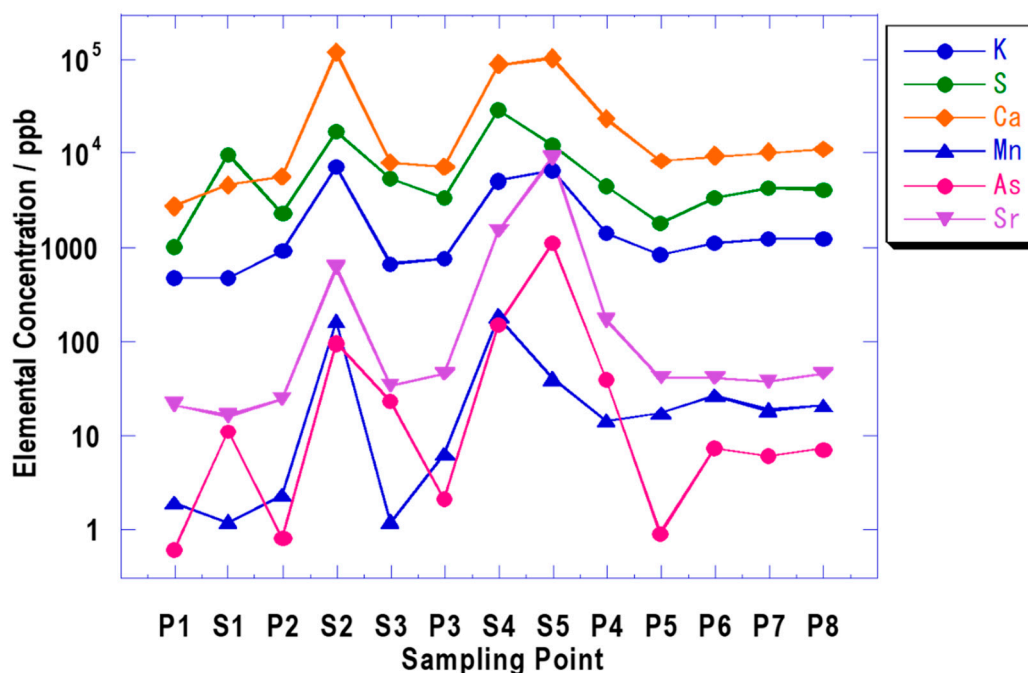


Figure 7. PIXE spectrum of airborne dust in Sapporo, Japan in April of 1982.

Many iron elements were observed in this spectrum. These were iron particulates from studded tires, which resulted in the prohibition of such tires.

#### 4. River Water

In the PIXE analysis of sea water, E.M. Johansson and S.A.E Johansson observed 28 elements in a sample taken from the sea in Sweden by applying a condensation method using a charcoal filter [25]. We analyzed river water using a condensation method based on colloids and precipitation. Figure 8 shows the results of the PIXE analysis of the river water sampled at eight points from the upper stream to the lower stream of the Miyagi Natori river [31]. S represents the hot spring water, which flows into the river, and P is the river water.



**Figure 8.** Quantities of elements contained in the water of the Natori river as a function of the sample position.

We can see that the arsenic discharged from the hot spring was immediately diluted by the river water.

#### 5. Archeological Sample

The difference between the PIXE analysis method and other analysis methods is that the distributions of elements are obtained by scanning particle beams on the surface of the sample. Since the space distributions of elements can be displayed as a picture, we call this a “PIXE camera.” Because the beam from the electrostatic accelerator has a very small emittance, a beam spot of 0.1 to 0.5 mm can be obtained by passing the beam through two narrow slits separated by a distance of approximately 1.5 m. The space distribution of each element is obtained by scanning beams on the sample with a dipole magnet and recording the detection position and energy of the X-ray [32]. Figure 9 shows a photograph of earthenware depicting a human face, which was discovered at the ruins of the Miyagi Kamikawana shell mound (approximately 7,000 years ago). The right side of the photo shows the distributions of Ca and Fe around an eye captured by a PIXE camera. It is believed that Ancient Japanese people (Jomon) had the custom of painting around the eyes with red iron oxide, like American indigenous peoples.

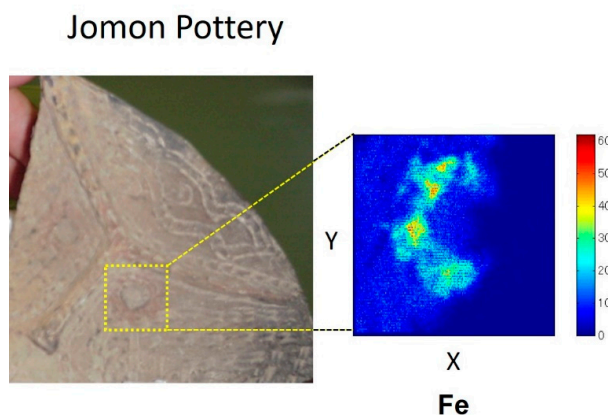


**Figure 9.** Spatial distributions of Ca and Fe from earthenware depicting a human face.

### 6. Elemental Analysis for Micron Area

By focusing beams to a diameter of within 1  $\mu\text{m}$ , intracellular element distributions can be obtained as a picture. A micro-beam smaller than 1.0  $\mu\text{m}$  diameter can be formed by the use of an electrostatic accelerator. A micro slit system and strongly convergent magnet quadrupole doublet (or superconductivity solenoid) were assembled on a vibration isolation table with a length of several meters. A beam spot with a diameter of 0.5  $\mu\text{m}$  and beam current of 20 pA achieved 3 MeV protons. Figure 10 shows the spatial distributions of potassium, sulfur, phosphorus, and bromine in the endothelial cells of a cow’s blood vessel, which was obtained by using a micro-PIXE camera at the Japan Atomic Energy Research Institute Takasaki research institute TIARA [33]. Phosphorus is concentrated in the nucleus. Bromodeoxyuridine is used in DNA synthesis. Since bromodeoxyuridine is integrated in the nucleus, it is used to determine the position thereof. The bromine is present due to the bromodeoxyuridine taken up by the nucleus.

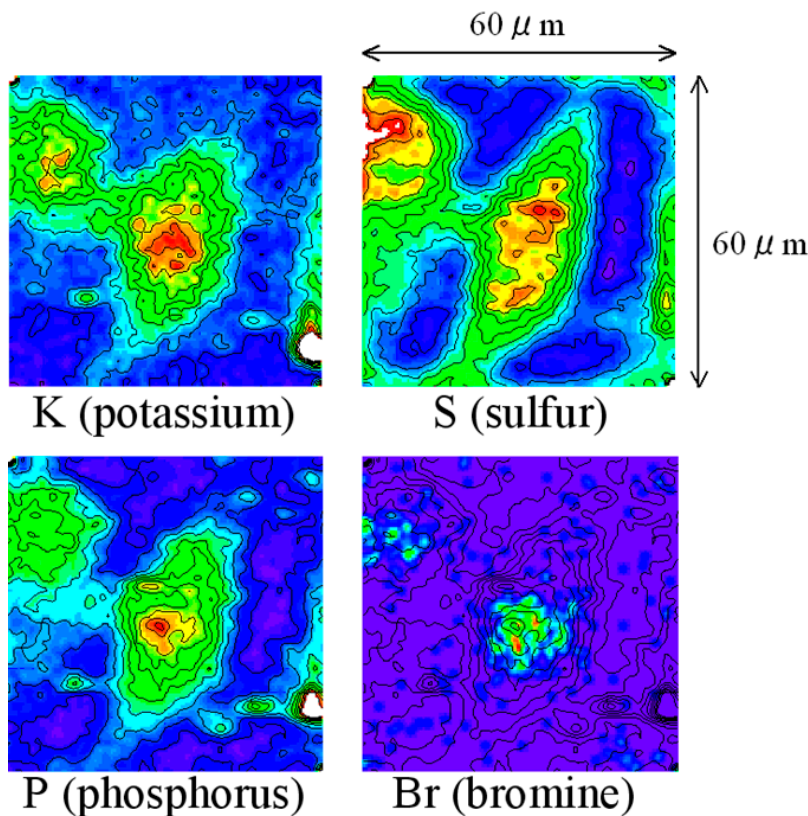


**Figure 10.** Elemental distributions of the endothelial cells of a blood vessel from a cow, obtained using a micro-PIXE camera with 2.6 MeV protons.

According to the results of micro-PIXE analysis of human esophageal cancer cells grown in culture solution containing cisplatin, Pt from cisplatin was detected in cancer cells [34]. This shows that the conformity of antineoplastic drugs can be investigated with in vitro experiments using micro-PIXE analysis.

The first task after the accident at the Fukushima Daiichi nuclear power plant was to quantify food contamination by radioisotopes. Small parts of brown rice harvested in Fukushima in the autumn of 2011 were polluted with radioactive cesium, which was problematic because the specific activity of a few sections of this small part exceeded the standard value (500 Bq/kg at this time and 100 Bq/kg thereafter in 2012). However, by polishing the contaminated brown rice, the specific activity of polished rice, which is white rice, decreased to below the standard value. Then, we grew rice in soil containing cesium and subjected a section of the brown rice to micro-PIXE analysis [35]. The results are shown in Figure 11.

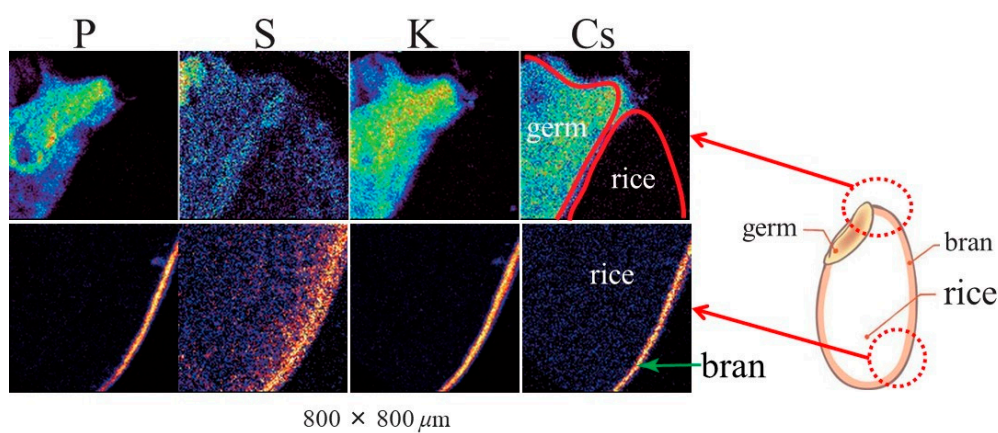


**Figure 11.** Distributions of elements in brown rice grains grown in soil containing cesium.

This figure confirms that cesium is concentrated in the bran and the germ. It was not contained in the rice.

## 11. Summary

The method of PIXE analysis is now a sufficiently sophisticated technology and is highly suitable for the analysis of biological, medical, and environmental samples. Therefore, our hope is that the general public will be able to use PIXE analysis freely. However, not so many accelerators can be applied to PIXE analysis. On the other hand, there are now many cyclotron accelerators of proton energy fixed in the range 10–20 MeV for cancer and brain diagnosis using positron emission tomography (PET). For example, there are 151 in Japan. Though the sensitivity of PIXE analysis using such high energy protons is not as high as mentioned at the end of Section 5, the promotion of the use of these accelerators to PIXE analysis will contribute to the development of this field.

**Funding:** This research received no external funding.

**Conflicts of Interest:** The author declare no conflict of interest.

## References

1. Johansson, T.B.; Akselsson, R. SAE Johansson X-ray analysis: elemental trace analysis at the 10–12 g level *Nucl. Instr. Meth.* **1970**, *84*, 141–143. [[CrossRef](#)]
2. Haraguchi, H.; Inagaki, K. Analysis for Environmental Monitoring: Analysis of Sediment, River Water and Seawater Samples by ICP-MS and ICP-AES. *Bunseki* **1998**, *7*, 494.
3. Johansson, S.A.E.; Campbell, J.L. *PIXE. A Novel Technique for Elemental Analysis*; John Wiley & Sons: Hoboken, NJ, USA, 1988.

4. Garcia, J.D. Inner-shell ionizations by proton impact. *Phys. Rev. A* **1970**, *1*, 280–285. [[CrossRef](#)]
5. Hansteen, J.M.; Mosebekk, O.P. Atomic Coulomb excitation by heavy charged particles. *Nucl. Phys. A* **1973**, *201*, 541–560. [[CrossRef](#)]
6. Lewis, H.W.; Simmon, B.E.; Merzbacher, E. Production of characteristic X-rays by protons of 1.7-to 3-Mev energy. *Phys. Rev.* **1953**, *91*, 943. [[CrossRef](#)]
7. Brandt, W.; Laubert, R.; Sellin, I. Characteristic X-ray Production in Magnesium, Aluminum, and Copper by Low-Energy Hydrogen and Helium Ions. *Phys. Rev.* **1966**, *151*, 56. [[CrossRef](#)]
8. Brandt, W.; Lapiki, G. Energy-loss effect in inner-shell Coulomb ionization by heavy charged particles. *Phys. Rev. A* **1981**, *23*, 1717. [[CrossRef](#)]
9. Cohen, D.D.; Harrigan, M. K-and L-shell ionization cross sections for protons and helium ions calculated in the ECPSR theory. *At. Data Nucl. Data Tables* **1985**, *33*, 255. [[CrossRef](#)]
10. Paul, H.; Sacher, J. Fitted empirical reference cross sections for K-shell ionization by protons. *At. Data Nucl. Data Tables* **1989**, *42*, 105. [[CrossRef](#)]
11. Scofield, J.H. Radiative Decay Rates of Vacancies in the K and L Shells. *Phys. Rev.* **1969**, *179*, 9. [[CrossRef](#)]
12. Bambynek, W.; Crasemann, B.; Fink, R.W.; Freund, H.V.; Mark, H.; Swift, C.D.; Price, R.W.; Rao, P.V. X-ray fluorescence yields, Auger, and Coster-Kronig transition probabilities. *Rev. Mod. Phys.* **1972**, *44*, 716. [[CrossRef](#)]
13. Kamiya, M.; Kinefuchi, Y.; Endo, H.; Kuwako, A.; Ishii, K.; Morita, S. Projectile-energy dependence of  $L\alpha$  to  $L_I$  x rays produced by proton and  $^3\text{He}$  impacts on Ho and Sm. *Phys. Rev. A* **1979**, *20*, 1820. [[CrossRef](#)]
14. Yamadera, A.; Ishii, K.; Sera, K.; Sebata, M.; Morita, S. Quasifree-electron bremsstrahlung induced by the projectile field. *Phys. Rev. A* **1981**, *23*, 24–33. [[CrossRef](#)]
15. Ishii, K.; Morita, S.; Tawara, H. Bremsstrahlung induced by proton and  $^3\text{He}$ -ion bombardments in the 1-4-MeV/amu energy range. *Phys. Rev. A* **1976**, *13*, 131–138. [[CrossRef](#)]
16. Ishii, K.; Morita, S. Continuum x rays produced by light-ion—atom collisions. *Phys. Rev. A* **1984**, *30*, 2278–2286. [[CrossRef](#)]
17. Johansson, S.A.E.; Campbell, J.L. *PIXE. A Novel Technique for Elemental Analysis*; John Wiley & Sons: Hoboken, NJ, USA, 1988; p. 288.
18. Ishii, K.; Morita, S. Theoretical estimation of PIXE detection limits. *Nucl. Instr. Meth. B* **1988**, *34*, 209–216. [[CrossRef](#)]
19. Ishii, K.; Morita, S. Bio-PIXE at the Takizawa facility (Bio-PIXE with a baby cyclotron). *Int. J. PIXE* **1990**, *1*, 1–29. [[CrossRef](#)]
20. Sera, K.; Yanagisawa, T.; Tsunoda, H.; Futatsugawa, S.; Hatakeyama, S.; Saitoh, Y.; Suzuki, S.; Orihara, H. Design of an ultra compact cyclotron for particle induced X-ray emission. Design of an ultra compact cyclotron for particle induced X-ray emission. *Int. J. PIXE* **1992**, *3*, 325. [[CrossRef](#)]
21. Wakasa, S.; Fukuda, K.; Takagi, T.; Nakanishi, N. Design of an ultra compact cyclotron for particle induced X-ray emission. *Int. J. PIXE* **1993**, *3*, 329–333. [[CrossRef](#)]
22. Ishii, K.; Terakawa, A.; Ushijima, H.; Hitomi, K.; Nagano, N.; Nogami, M. Application of a medical PET cyclotron to PIXE Analysis. In Proceedings of the 16th International Conference on Particle Induced X-ray Emission, Caldas da Rainha, Portugal, 24–29 March 2019; Volume 39. Available online: [https://i.pixe2019.org/event/1/attachments/1/15/PIXE2019\\_book\\_abstracts.pdf](https://i.pixe2019.org/event/1/attachments/1/15/PIXE2019_book_abstracts.pdf) (accessed on 21 April 2019).
23. Ishii, K.; Orihara, H.; Iwata, Y.; Bessho, K. Detection limit for a very thin backing film. *Int. J. PIXE* **1994**, *4*, 1–7. [[CrossRef](#)]
24. Futatukawa, S. Bio PIXE Theory and Applications. Chapter 2. Sample Preparation for the Quantitative Analysis of Biological Materials. (1) Sample Preparation Method of Biological Materials by Nitric Acid Ashing Using a Microwave Oven. *Radioisotopes* **2000**, *49*, 447–450. Available online: <https://doi.org/10.3769/radioisotopes.49.447> (accessed on 21 April 2019).
25. Johansson, E.M.; Johansson, S.A.E. PIXE analysis of water at the parts per trillion level. *Nucl. Instr. Meth. B* **1984**, *3*, 154–157. [[CrossRef](#)]
26. Mandó, P.A. Advantages and limitations of external beams in applications to arts & archeology, geology and environmental problems. *Nucl. Instr. Meth. B* **1994**, *85*, 815–823.
27. Murozono, K.; Ishii, K.; Yamazaki, H.; Matsuyama, S.; Iwasaki, S. PIXE spectrum analysis taking into account bremsstrahlung spectra. *Nucl. Instr. Meth. Phys. Res. B* **1999**, *150*, 76–82. [[CrossRef](#)]

28. Ishii, K.; Morita, S.; Tawara, H.; Chu, T.C.; Kaji, H.; Shiokawa, T. Quantitative trace-element analysis by proton-induced X-rays. *Nucl. Instr. Meth.* **1975**, *126*, 75–80. [[CrossRef](#)]
29. ISHII, K.; Morita, S. Present state of Bio-PIXE. *Radioisotopes* **1993**, *42*, 579–589. [[CrossRef](#)]
30. Mohri, M.; Amemiya, S.; Maeda, S.; Fukuda, S.; Kato, S.; Satake, T.; Hashiba, M.; Yamashina, T. *Bulletin of the Faculty of Engineering*; Hokkaido University: Hokkaido, Japan, 1983; Volume 114, pp. 47–56.
31. Yamazaki, H.; Tanaka, M.; Tsutsumi, K.; Ishii, K.; Iwasaki, S.; Matsuyama, S.; Inoue, J.; Murozono, K.; Orihara, H. Determination of heavy-metal concentrations in water by PIXE analysis using Zr as an internal standard. *Int. J. PIXE* **1997**, *7*, 31–43. [[CrossRef](#)]
32. Matsuyama, S.; Gotoh, K.; Ishii, K.; Yamazaki, H.; Satoh, T.; Yamamoto, K.; Sugimoto, A.; Tokai, Y.; Endoh, H.; Orihara, H. Development of a submilli-PIXE camera. *Int. J. PIXE* **1998**, *8*, 209–216. [[CrossRef](#)]
33. Ishii, K.; Sugimoto, A.; Tanaka, A.; Satoh, T.; Matsuyama, S.; Yamazaki, H.; Akama, C.; Amartivan, T.; Endoh, H.; Oishi, Y.; et al. Elemental analysis of cellular samples by in-air micro-PIXE. *Nucl. Instr. Meth. B* **2001**, *181*, 448–453. [[CrossRef](#)]
34. Tanaka, N.; Kimura, H.; Asao, T.; Kuwano, H.; Sakai, T.; Oikawa, M.; Satoh, T.; Kamiya, T. Investigation of Cisplatin Sensitivity in Esophageal Squamous Cancer Cell Lines and the Localization of Pt Using In-air Micro-PIXE. *JAEA-Rev.* **2007**, *060*, 131. Available online: <https://jopss.jaea.go.jp/pdfdata/JAEA-Review-2007-060.pdf> (accessed on 21 April 2019).
35. Koshio, S.; Ishii, K.; Matsuyama, S.; Terakawa, A.; Fujiwara, M.; Watanabe, K.; Oshikawa, S.; Kikuchi, K.; Itoh, S.; Kasahara, K.; et al. Measurement of distributions of cesium and rubidium in rice grains using micro-PIXE for detailed examinations of contaminated food. *Int. J. PIXE* **2014**, *24*, 15. Available online: <https://doi.org/10.1142/S0129083514500028> (accessed on 21 April 2019).



© 2019 by the author. Licensee MDPI, Basel, Switzerland. This article is an open access article distributed under the terms and conditions of the Creative Commons Attribution (CC BY) license (<http://creativecommons.org/licenses/by/4.0/>).